Explaining an Unusually Fast Parasitic Enzyme: Folate Tail-Binding Residues Dictate Substrate Positioning and Catalysis in *Cryptosporidium hominis* Thymidylate Synthase[†,‡]

W. Edward Martucci,[§,||] Melissa A. Vargo,[||] and Karen S. Anderson*[,||]

Department of Molecular Biophysics and Biochemistry and Department of Pharmacology, Yale University School of Medicine, 333 Cedar Street, New Haven, Connecticut 06520

Received March 18, 2008; Revised Manuscript Received June 30, 2008

ABSTRACT: The essential enzyme TS-DHFR from *Cryptosporidium hominis* undergoes an unusually rapid rate of catalysis at the conserved TS domain, facilitated by two nonconserved residues, Ala287 and Ser290, in the folate tail-binding region. Mutation of these two residues to their conserved counterparts drastically affects multiple steps of the TS catalytic cycle. We have determined the crystal structures of all three mutants (A287F, S290G, and A287F/S290G) in complex with active site ligands dUMP and CB3717. The structural data show two effects of the mutations: an increased distance between the ligands in the active site and increased flexibility of the folate ligand in the partially open enzyme state that precedes conformational change to the active catalytic state. The latter effect is able to be rescued by the mutants containing the A287F mutation. In addition, the conserved water network of TS is altered in each of the mutants. The structural results point to a role of the folate tail-binding residues in closely positioning *Ch*TS ligands and restricting ligand flexibility in the partially open state to allow for a rapid transition to the active closed state and enhanced rate of catalysis. These results provide an explanation on how folate tail-binding residues at one end of the active site affect long-range interactions throughout the TS active site and validate these residues as targets for species-specific drug design.

Thymidylate synthase (TS)[1] is an essential enzyme in all organisms, catalyzing the *de novo* synthesis of deoxythymidine monophosphate (dTMP) from deoxyuridine monophosphate (dUMP), and as such has long been used as a chemotherapeutic target for cancer and infections. During the step of methyl transfer to dUMP, TS utilizes the folate cofactor 5,10-methylenetetrahydrofolate (CH_2H_4folate), making the partially reduced dihydrofolate (H_2folate) in the process (*1*). The dihydrofolate product is used by dihydrofolate reductase (DHFR), with nicotinamide adenine dinucleotide phosphate (NADPH), to produce the reduced folate, tetrahydrofolate (H_4folate) (*2*). Tetrahydrofolate is used as a source of one-carbon unit transfers in multiple biological processes, including dTMP and purine nucleotide biosynthesis, and synthesis of glycine and methionine. Thymidylate synthase is a highly conserved enzyme across all species in overall structure on the residue level at the active site (*1*).

While TS and DHFR are expressed as separate monofunctional enzymes in humans and most other species (*1*), in protozoan parasites the two catalytic activities exist as one bifunctional enzyme, residing on the same polypeptide chain (*3*). The thymidylate synthase domain of bifunctional thymidylate synthase−dihydrofolate reductase (TS-DHFR)[2] from the protozoan parasite *Cryptosporidium hominis* is a unique enzyme with an unusually rapid rate of catalysis, roughly 10−40-fold faster than almost all other species of the enzyme (*4*). Considering the highly conserved nature of this enzyme, it was surprising to find such a difference. In the active site, two residues residing on the folate tail-binding helix, Ser290[3] and Ala287, differ from the usual eukaryotic conserved residues at those positions: a glycine and phenylalanine, respectively (*5*). Kinetic analysis previously pinpointed these residues as effecting the large rate increase in *Ch*TS-DHFR; when the residues were mutated to their more common counterparts, there was a large decrease in activity, as shown in Table 1 (*6*). Structural data from the S290G mutant pointed for a role in substrate positioning, however was unable to explain how the mutants with the A287F

[†] This work was supported in part by NIH Grant AI 44630 (to K.S.A.) and NIH Grant 5T32-AI 07404 (to W.E.M.).

[‡] The coordinates for the structures reported in this work have been deposited in the Protein Data Bank under the following file names: A287F, 3DL5; S290G, 2OIP; A287F/S290G, 3DL6.

* To whom correspondence should be addressed. Telephone: (203) 785-4526. Fax: (203) 785-7670. E-mail: karen.anderson@yale.edu.

[§] Department of Molecular Biophysics and Biochemistry, Yale University School of Medicine.

[||] Department of Pharmacology, Yale University School of Medicine.

[1] Abbreviations: TS, thymidylate synthase; DHFR, dihydrofolate reductase; *Ch*, *Cryptosporidium hominis*; dUMP, deoxyuridine monophosphate; dTMP, deoxythymidine monophosphate; CB3717, 10-propargyl-L-5,8-dideazafolate; CH_2H_4folate, methylenetetrahydrofolate.

[2] TS-DHFR, thymidylate synthase−dihydrofolate reductase is a functional designation as catalysis at TS precedes catalysis at DHFR; elsewhere, the bifunctional enzyme is called DHFR-TS based on DHFR being N-terminal to TS (*3*).

[3] The amino acid numbering sequence used is that of *C. hominis* TS-DHFR. The *E. coli* TS numbering of the more important residues in this paper is as follows: *C. hominis* Ala287 = *E. coli* His51; Ser290 = Gly54; Ile315 = Ile79; Phe433 = Phe176.

10.1021/bi800466z CCC: $40.75
Published on Web 08/02/2008

Table 1: Values for k_{cat}, Efficiency, and Single-Enzyme Turnover[a]

	k_{cat} (s^{-1})	efficiency, k_{cat}/K_m (μM^{-1} s^{-1})	single-enzyme turnover (s^{-1})
WT	11.7 ± 0.2	4.3	27.3 ± 0.5
A287F	8.2 ± 0.3	0.81	13.5 ± 0.9
S290G	0.8 ± 0.2	0.02	2.3 ± 0.1
A287F/S290G	7.6 ± 0.3	0.87	13.6 ± 0.7

[a] From ref *6*.

mutation could partially rescue many of the kinetic defects of the S290G enzyme.

The crystal structure of *Ch*TS-DHFR shows a clear hydrogen bond between Ser290 and the glutamate tail of the antifolate CB3717 (*7*), and previous work has implicated that residues in the folate tail-binding region, including the conserved phenylalanine at position 287, are important for folate binding (*8, 9*). It is known that species differences at both positions 287 and 290 lead to altered antifolate drug specificity, and this region has been identified as a target for species-specific drug design (*10, 11*). However, there is a lack of information on how this region, far from the site of methyl transfer, impacts catalysis. A full understanding of how these residues impact catalysis is necessary, as there are currently no antiparasitic drugs available for the treatment of cryptosporidiosis, the disease caused by *C. hominis* (*12*).

In this study, we have attempted to gain insight into the physical mechanism by which Ala287 and Ser290 influence rapid catalysis at the unusually fast *C. hominis* TS domain and how Phe287 is able to partially rescue the Ser290 mutation. We have determined the X-ray crystal structure of three *Ch*TS-DHFR "revertant mutant" enzymes: the severely impaired S290G (*6*), and the two moderately affected enzymes, A287F and double mutant (A287F/S290G). Coupled with the previously reported kinetic data, the structures reported here offer a physical description of how residues at the folate tail-binding region of the active site modulate substrate positioning and flexibility through long-range effects. The results provide a better understanding of how the enhanced catalytic rate at *Ch*TS is achieved and validate the species-unique tail-binding residues as possible target sites for species-specific inhibitor development.

MATERIALS AND METHODS

Chemicals and Reagents. All buffers and other reagents used were of the highest commercial purity. Millipore ultrapure water was used for all solutions. 7,8-Dihydrofolate (H_2folate) was chemically prepared by the reduction of folate with sodium hydrosulfite.

*Protein Expression and Purification. Ch*TS-DHFR was purified as previously published (*4*). Site-directed mutations were created using a QuikChange mutagenesis kit (Stratagene). Plasmids containing the desired mutations, as confirmed by nucleic acid sequencing, were used to transform competent *E. coli* BL21-DE3 cells, and proteins were purified in a manner similar to wild-type. After elution from the resin, the purified proteins were concentrated to levels suitable for crystallization.

Crystallization and Data Collection. Pure *Ch*TS-DHFR mutant protein was incubated at a final concentration of 7 mg/mL with 1 mM ligands (dUMP, CB3717 (a kind gift from Dr. Ann Jackman, The Institute of Cancer Research, Sutton, U.K.), NADPH, and methotrexate) for 45 min on ice. The protein/ligand mix was crystallized using the hanging-drop vapor diffusion technique. The successful well solution for S290G was 0.1 mM ammonium sulfate, 0.3 M lithium sulfate, 0.1 M Tris, and 10% polyethylene glycol 6000. A287F crystallization was successful under the following conditions: 0.1 mM ammonium sulfate, 0.25 M lithium sulfate, 0.1 M Tris, and 11% polyethylene glycol 6000. A287F/S290G crystallization was successful under the following conditions: 0.05 mM ammonium sulfate, 0.15 M lithium sulfate, 0.1 M Tris, and 11% polyethylene glycol. Crystals of approximate dimensions 0.3 mm × 0.1 mm × 0.05 mm grew in 1 week at 18 °C for all three mutant proteins. Crystals were soaked in successive cryoprotectants of mother liquor plus 10%, 15%, and 25% ethylene glycol for 2 min each and were flash frozen in liquid nitrogen.

Diffraction data were collected at Brookhaven National Laboratory at beam lines X25 (S290G and A287F) and X29 (A287F/S290G). Data were indexed, integrated, and scaled using the HKL2000 software (*13*) and were converted to structure factors with the program Truncate (*14*). Five percent of reflections were marked for cross-validation analysis to serve as R_{free}. The structure of the WT *Ch*TS-DHFR enzyme was solved on similar instruments at the same facility and scaled and refined using the same software, allowing us to make comparisons between the WT structure and the ones presented here.

Structure Solution. The structures of *Ch*TS-DHFR mutant proteins cocrystallized with ligands were all solved using the coordinates of wild-type *Ch*TS-DHFR (Protein Data Bank 1QZF), with waters and ligands removed, as a starting model. All of the proteins crystallized with approximately the same space group and unit cell as wild-type, allowing direct refinement against the starting model. A rigid-body fit using Refmac5 from the CCP4 suite was performed, followed by a refinement in which the domains were allowed to move independently (*15*). Mutations were built into the model, and the structures were refined using Refmac5, with density modification conducted using solvent flipping in Solomon (*14, 15*), and iterative processes of refinement and manual residue and ligand positioning were carried out in the visualization programs O (*16*) and COOT (*17*). Waters were added using Refmac5, and either *B*-factors or group *B*-factors were refined in CNS for the S290G and A287F structures and the A287F/S290G double mutant structure, respectively (*18*). The same procedure, type, and order of refinement programs were kept consistent between structures so that they would be directly comparable. All refinement statistics are reported in Table 2.

RESULTS

X-ray Crystal Structure Solution of the TS Mutant Enzymes. In order to assess the physical impact of the mutations associated with decreased catalytic rate, we determined the X-ray crystal structure of three active site mutants of *Ch*TS-DHFR: the S290G and A287F single mutants and the A287F/S290G double mutant. For direct comparison with the wild-type *Ch*TS-DHFR structure (*7*), the same TS ligands (dUMP and CB3717) and DHFR ligands (NADPH and methotrexate) were cocrystallized with the enzymes. The inhibitor CB3717 at the TS domain has been validated to serve as an accurate

Table 2: Data Collection and Refinement Statistics for Structures of *Ch*TS-DHFR Mutants Complexed with dUMP, CB3717, NADPH, and MTX/DHF[a]

	S290G (*6*)	A287F	A287F/S290G
Crystal Data			
resolution limit (Å)	2.80	2.74	3.25
space group	*C*2	*C*2	*C*2
unit cell parameters			
a, *b*, *c* (Å)	215.0, 116.2, 216.6	215.3, 116.2, 219.3	214.9, 116.9, 220.9
β (deg)	94.27	95.16	94.94
no. of reflections used	130114	144384	83352
completeness (%)	99.2 (98.7)	99.8 (99.8)	98.2 (84.8)
redundancy	3.3	3.6	3.5
$I/\sigma I$	9.3 (2.9)	9.5 (2.1)	8.8 (1.9)
R_{merge} (%)	11.7 (53.8)	12.3 (68.2)	10.6 (48.4)
Refinement Statistics			
R_{factor} (%)	22.1	21.4	22.5
R_{free} (%)	26.0	24.5	27.6
total no. of atoms	21926	21793	21446
no. of water molecules	399	521	143
rmsd, bonds (Å)	0.009	0.008	0.009
rmsd, angles (deg)	1.4	1.4	1.5
average *B*-factor, TS dimer (Å^2) (monomers A and B)	46	41	53
average *B*-factor, total protein (Å^2)	66	53	64
average *B*-factor, waters (Å^2)	60	48	60
Wilson *B* (Å^2)	72	68	49
Ramachandran Plot Statistics			
residues in most favored (%)	88.3	89.1	81.9
residues in additionally allowed (%)	10.9	10.5	17.1
residues in generously allowed (%)	0.7	0.3	0.9
residues in disallowed (%)	0.1	0.1	0.0

[a] Values in parentheses are for the highest resolution shell.

model for the TS mechanism (*19*), and methotrexate has been shown to bind DHFR in its structural "transition state" (*20*). All three enzymes crystallized in the same space group and roughly the same asymmetric unit as wild-type *Ch*TS-DHFR, with 5 subunits (2.5 dimers) per unit, allowing us to proceed directly to refinement using the wild-type structure (PDB ID: 1QZF) as a good starting model. In all of the enzymes, monomers A and B form a dimer, C and D form a dimer, and E forms a dimer across the crystallographic 2-fold axis.

The electron density for backbone atoms was complete for all monomers. For all three data sets, the electron density for monomers D and E was less well defined than in A, B, and C. Noncrystallographic symmetry was not used, as the thymidylate synthase enzyme has been shown to be half-the-sites reactive, and two monomers within a dimer can display slight structural differences related to catalysis (*21, 22*). Most side chain electron density was visible for all monomers, with the exception of the flexible linker loop. Roughly, residues 180−190 of each monomer were omitted, with an additional ~3 residues built as alanines. In the initial maps, there was clear positive difference density for residue 287 and negative difference density for residue 290 at 3σ in the mutated structures, allowing the placement of the mutated side chains directly after initial refinement. The electron density for all ligands was complete in monomers A and B for all three structures, with the exception of the Cβ−Cγ bond of the folate tail of CB3717 in the S290G enzyme. However, carboxylate density allowed proper positioning of the folate tail. Representative $F_o - F_c$ difference maps for ligands in the three mutants are shown in Figure 1. Although the resolution of the double mutant was lower than the other structures, and therefore the errors in atom position slightly higher, the inclusion of that mutant is important to independently validate the results seen with the single mutants.

Position of Mutated Residues 287 and 290. The position of each mutated side chain had clear, visible difference electron density for each mutant enzyme in the early stages of refinement. The mutants with a glycine replacing a serine at position 290 show that the backbone atoms are unchanged from wild-type. However, there is a difference for the two structures in which Ala287 was mutated to a phenylalanine. In the A287F/S290G double mutant, the Phe287 occupies a space below the CB3717 folate tail, partially occupying the van der Waals space of Ser290 from WT (Figure 2A). This conformation is the typical positioning of Phe287 in most TS species, which also typically have a glycine at position 290. In stark contrast is the position of Phe287 in A287F, in which the phenylalanine ring occupies space above the folate tail (Figure 2A). When Ser290 occupies the space below the folate tail, the phenylalanine ring cannot and is forced to adopt a different rotamer, rotated nearly 180°. To our knowledge, this rotamer has never been identified for a traditional TS species containing a phenylalanine at that position. In both of our mutant structures containing a phenylalanine, regardless of its position the phenylalanine interacts with and appears to order the carboxylate moiety of the folate tail (Figure 2B). The conformation is interesting, in that the carboxylate−aromatic interaction appears less like the common edgewise arrangement (*23*) and more resembles carbonyl−nucleotide stacking (*24*).

Comparison of TS Mutant and WT Tertiary Structures. A comparison of the overall tertiary structures of a single TS domain from wild-type, S290G, A287F, and A287F/S290G showed there are no major changes in the structures of the mutant proteins. A least-squares alignment of Cα atoms was done using LSQKAB in which every combination of monomers A and B from all four structures was compared and revealed that no alignment had an rmsd greater than 0.28 Å (*14*). In each mutant enzyme, the helix on which residues 287 and 290 reside remains fully helical and in the same orientation toward the active site as in the wild-type enzyme.

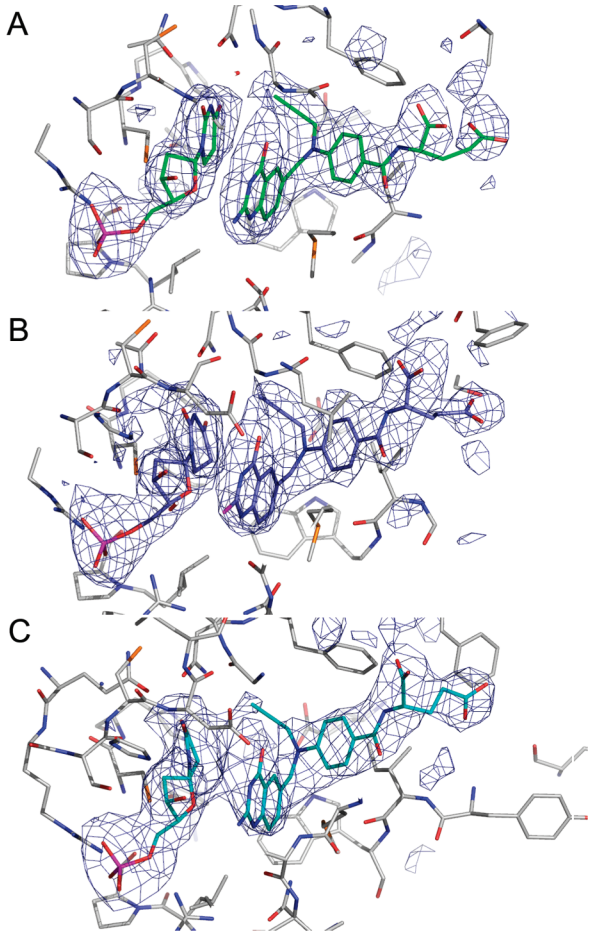

FIGURE 1: Initial $F_o - F_c$ difference density maps of the monomer B active sites of (A) S290G, (B) A287F, and (C) A287F/S290G mutant enzymes. Maps are contoured at 2.5σ and show clearly defined density for the ligands, with the exception of the C−C bond of the glutamate tail of CB3717 in S290G and the propargyl carbons 1 and 2 in A287F/S290G.

The two monomers with the best overall electron density, A and B, form a biological dimer. Thymidylate synthase dimers are known to be half-the-sites reactive, and TS crystal structures have shown asymmetry of the monomers, with one in a more closed and active conformation and the other in a more open conformation with higher disorder of the ligands (*21, 25, 26*). While the overall tertiary structure of the A and B monomers in all of our mutant enzymes was similar, the A subunit had a more open conformation, as evidenced by the closing of Tyr466 on the active site, slightly altered position of dUMP, as well as the expected increase in ligand *B*-factors.

Comparison of TS Mutant and WT Ligand Orientation. A comparison of the TS active sites at the residue level showed that there are only small changes to side chains of residues in the active site. There are, however, significant changes in the position of the two ligands in the active site and their orientation with respect to one another.

In S290G, the most severely impaired mutant, the folate tail of CB3717 is moved away from the folate tail-binding helix and down in the active site compared to wild-type (Figure 3). This seems to lead to significant changes in the overall position of the ligands. The largest change comes from the Cα of the folate tail, which moves by over 1.3 Å, and the entire compound is shifted up and away from its position in WT, by about 0.8 Å at most atom positions. The dUMP substrate at the far side of the active site is also altered. A possible hydrogen bond between the two substrates is lost in S290G, as the distance between O3′ of dUMP and N3 of CB3717 is increased by over 1.0 Å, and the entire dUMP compound is shifted down and away from its wild-type position. Most importantly for catalytic implications, the largest distance increase between the two substrates is between the two atoms involved in the catalytic methyl transfer step, C5 of dUMP and CP1 of CB3717 (analogous to C10 in CH_2H_4folate). These two atoms increase by 1.3 Å, moving from 4.0 to 5.3 Å (Figure 3).

In A287F, in which the catalytic decrease is less dramatic, the folate tail of CB3717 is also shifted down from its position in WT, but the glutamate side chain of the tail adopts a unique orientation from both WT and S290G (Figure 3). The *p*-aminobenzoate moiety is also shifted. The rest of the CB3717 compound, however, aligns very closely with S290G, and the quinazoline head of the folate is pulled away from its position in WT to the same degree. The movements in dUMP are almost identical with S290G, and both the abolished hydrogen bond distance (3.7 Å) and catalytic atom distance (4.9 Å) are consistent with those seen for S290G (Figure 3).

The ligands in the double mutant (A287F/S290G) align very closely with those of the single mutant enzymes. Again, while the glutamate tail of CB3717 is shifted down from its position in WT and the side chain of the glutamate tail is in a unique conformation, the majority of the CB3717 compound overlays closely with the mutants, showing the same changes from WT (Figure 3). In the case of the double mutant, the dUMP pyrimidine ring is shifted more than either of the single mutants; however, the slight change in the position of the progargyl group of CB3717 keeps the catalytic atom distance similar to the other mutants, at 4.9 Å (Figure 3).

In addition to the catalytic distances discussed above, another distance pertinent to catalysis is that of catalytic Cys402 Sγ to C6 of dUMP. These two atoms form a covalent bond in the mechanistic step where the cysteine activates dUMP; however, this was not observed in any of the structures, WT or mutant. While there was a slight increase in distance between the two atoms in the mutant structures, it was not significant based on our coordinate errors.

Analysis of Protein−ligand Interactions. Since the ligand positioning was altered in all three active site mutants, we conducted an analysis of the protein−ligand interactions to determine if any were lost in the mutants that may explain the dramatic rate decrease. Shown in Table 3 are specific hydrogen bonds and hydrophobic contacts between the protein and the TS ligands dUMP and CB3717, as calculated by the program LIGPLOT (*27*). Hydrogen bonds were defined with a cutoff of 3.35 Å and hydrophobic contacts with a cutoff of 5.0 Å. The values reported are conservative, and though we acknowledge there may be some weaker interactions within error of the distances reported here, they give a generally low cutoff.

In addition to the obvious loss of the Ser290 hydrogen bond to the CB3717 folate analogue, the ligands in S290G lose two additional hydrogen bonds to residues in the active site: Cys402 Sγ (the catalytic cysteine in TS) to O4′ of dUMP and the backbone oxygen of Ala520 to CB3717 quinazoline

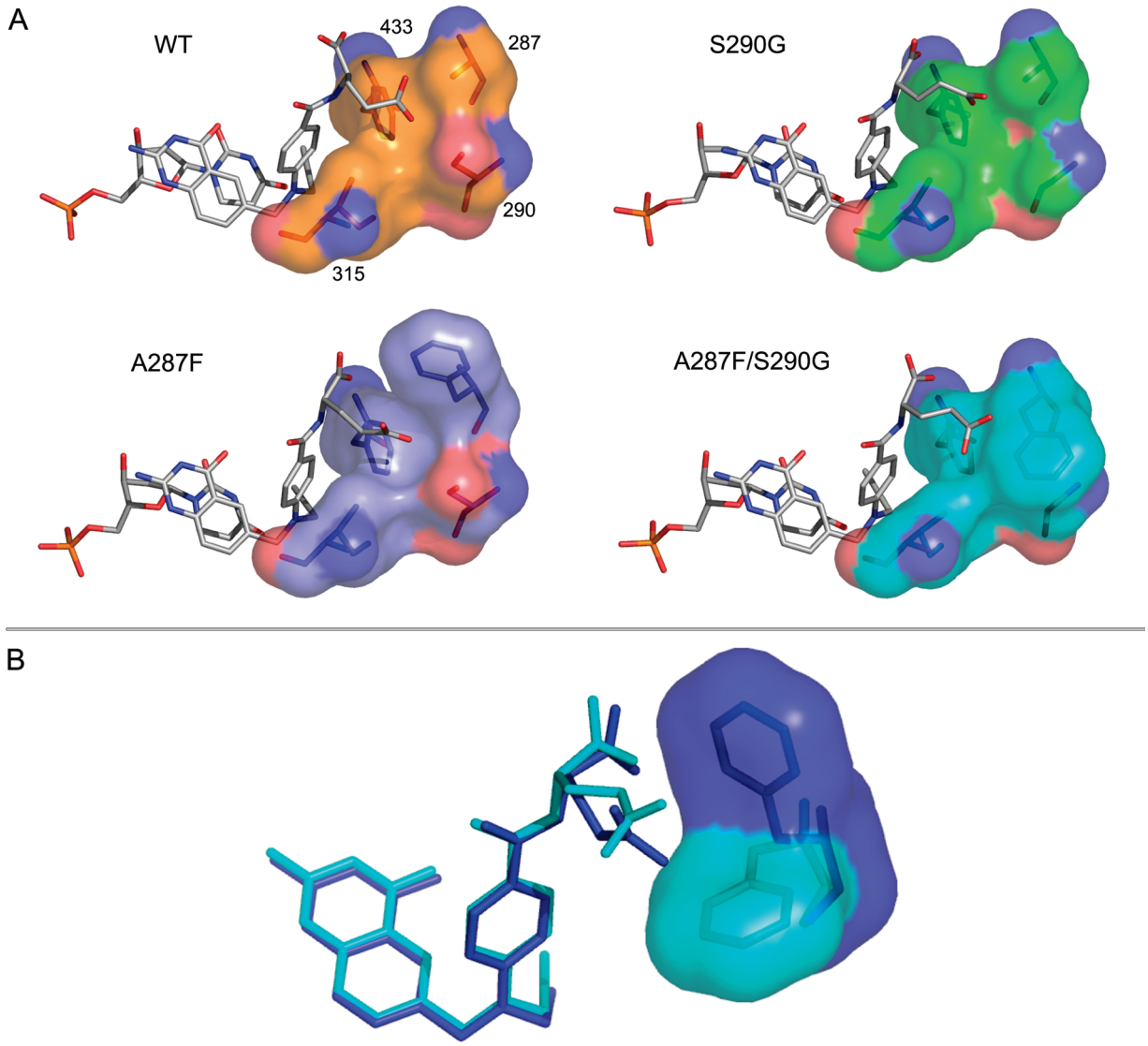

FIGURE 2: Folate tail-binding residues for each TS enzyme. (A) The four folate tail-binding residues Ala/Phe287, Ser/Gly290, Ile315, and Phe433 are shown as side chain sticks beneath their molecular surface, for WT from PDB 1QZF (orange) and each mutant enzyme: S290G (green), A287F (blue), and A287F/S290G (cyan). TS ligands are shown in gray. (B) Close-up view of an alignment of A287F (blue) with A287F/S290G (cyan), highlighting the difference in position of Phe287 and subsequent orientation of the CB3717 folate tail.

amine. The hydrogen bond interactions are lost in the more open monomer A. Interestingly, the other two hydrogen bonds lost reside on the opposite side of the active site from residue 290, highlighting the long-range effects of the mutation. The A287F and A287F/S290G mutants lose three total protein−ligand hydrogen bonds, one of which is Ser290, a noteworthy result considering that the Ser290 is not mutated in A287F.

Protein−ligand hydrophobic contacts were also analyzed. As with the hydrogen bond analysis, the S290G mutant enzyme loses a considerable number of hydrophobic contacts. In monomer B, four residues that make ligand contacts in WT no longer maintain interactions in S290G. The majority of lost interactions are from CB3717 (Ala287, Asn319, Leu399, Asn434), while only one interaction (Asn434) with dUMP is lost (Table 3). The more open monomer A for S290G showed all of these lost interactions, with an additional loss of Leu429 with CB3717.

There is a difference with less affected A287F and A287F/S290G mutants, as the open monomer A of both mutants regains the interaction with Leu429, and monomer B of both mutants additionally regains interactions with Leu399 with CB3717 and Asn 434 with dUMP (A287F) and CB3717 (A287F/S290G). (Table 3). The important difference from S290G is that both monomers from both enzymes recover the interaction of CB3717 with residue 287.

An additional point of emphasis for the interaction analysis is the extent of contact involved in each protein−ligand van der Waals interaction (Table 3). Whereas most of the interactions that are maintained from WT and mutants have the same degree of interaction, two residues in the open monomer A stand out in contrast. Ile315, one of the three residues that forms the folate tail-binding region (along with 287 and 290), actually involves a greater degree of interaction with CB3717 in monomer A of A287F and A287F/S290G mutant compared with monomer A in S290G and WT. Ile315 from A287F makes additional contacts with the benzoate ring while also utilizing its Cα in the interaction, which the other enzymes do not. Monomer B from the single mutant enzymes also

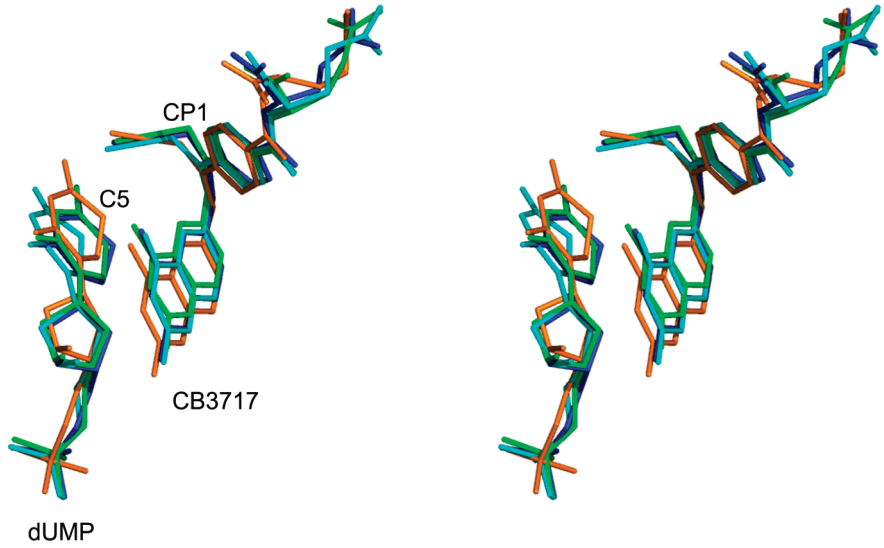

FIGURE 3: A stereo representation of the orientation of TS ligands in the active sites of wild-type and mutant enzymes. The ligands dUMP and CB3717 are shown from the structures of WT (orange), S290G (green), A287F (blue), and A287F/S290G (cyan). Note the changes in the position of dUMP, the quinazoline head of CB3717, and the folate tail.

Table 3: Protein−Ligand Hydrogen-Bonding and Hydrophobic Contacts for TS Monomers A and B of WT, S290G, and A287F[a]

hydrogen bond		distance (Å)							
		WT		S290G		A287F		double	
donor	acceptor	A	B	A	B	A	B	A	B
Ser290 Oγ	CB3717 Oϵ1	3.1	3.1			(3.7)	(3.7)		
Arg382 NH2	dUMP O2P	2.7	2.6	3.2	3.0	3.2	3.0	2.4	3.1
Arg382 Nϵ	dUMP O2P	2.5	2.6	3.0	3.3	3.3	3.2	2.9	2.4
Arg383 NH1	dUMP O1P	2.7	2.7	2.7	2.7	2.2	3.2	2.0	2.2
Cys402 Sγ	dUMP O4′	3.2	3.0	(3.9)	(4.0)	(4.0)	(4.1)	(4.0)	(3.6)
Arg423 NH2	dUMP O3P	3.0	2.8	3.3	2.9	2.6	2.8	3.3	2.9
Arg423 NH1	dUMP O3P	2.6	2.5	2.4	2.7	2.5	2.6	2.7	3.0
Asp426 N	dUMP O2	3.2	3.3	2.5	3.1	2.8	3.2	2.7	2.6
His464 Nϵ2	dUMP O3′	3.1	3.3	2.9	2.8	3.2	3.1	2.9	3.3
Tyr466 OH	dUMP O3′	2.9	3.1	2.5	2.7	2.6	2.9	2.3	2.3
dUMP N3	Asn434 Oδ1	2.4	2.4	3.0	3.1	3.1	3.1	3.1	2.6
CB3717 NA2	Ala520 O	2.8	2.9	(3.5)	(4.0)	(3.5)	(3.7)	(3.7)	(3.7)

		extent of interaction[b]							
		WT		S290G		A287F		double	
hydrophobic contact	hydrophobic contact	A	B	A	B	A	B	A	B
CB3717	Ala287 (Phe287)	+	+	−	−	+	+	+	+
CB3717	Ile315	++	++	++	+++	+++	+++	+++	++
CB3717	Asn319	+	+	−	−	−	−	−	−
CB3717	Leu399	+	+	−	−	−	+	−	+
dUMP	Cys402	++	+++	++	++	++	++	++	++
dUMP	Ser424	+	+	+	+	+	+	+	+
CB3717	Leu429	+	+	−	+	+	+	+	+
CB3717	Gly430	+	+	+	+	+	+	+	+
CB3717	Phe433	+++	+++	+	++	++	++	++	++
CB3717	Asn434	+	+	−	−	−	+	−	−
dUMP	Asn434	+	+	−	−	−	−	−	+
CB3717	Met519	++	++	++	+	++	+	++	++
CB3717	dUMP	+++	+++	++	+++	+++	++	++	++

[a] Values in parentheses do not satisfy the distance criteria for a hydrogen bond. [b] + = 1−4 atom interactions; ++ = 5−8 atom interactions; +++ = 9−12 atom interactions.

displays this increased extent of interaction, whereas monomer B of A287F/S290G does not. Additionally, Phe433, which maintains extensive contacts to the *p*-aminobenzoate phenyl ring in wild-type enzyme, contains only half of the interactions in A287F and A287F/S290G and is reduced to only a few atoms in S290G. Importantly, the overall movement of the ligands with respect to each other is highlighted by the fact that, in the WT structure, dUMP and CB3717 make 13 interligand hydrophobic contacts, versus an average of 7 contacts for the mutant enzymes.

In addition to interactions that were lost in the mutants, there are a few gained interactions as well. There are four hydrogen bonds gained in all of the mutant enzymes that are absent in WT: Arg257 to O5′ of dUMP, Ser424 to a dUMP phosphate oxygen, Asn434 to O4 of dUMP, and

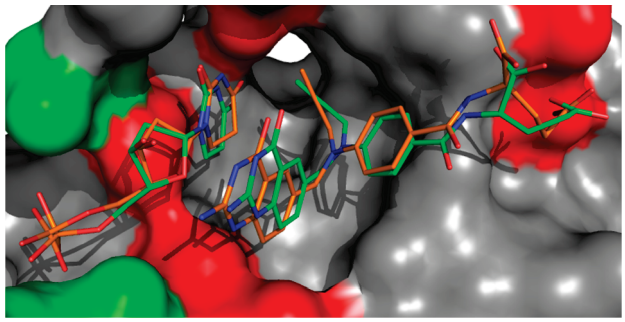

FIGURE 4: Lost and gained protein−ligand interactions for the S290G mutant enzyme. Molecular surface representation of the WT TS monomer B active site interactions lost (red) and gained (green) in the S290G mutant TS enzyme. WT ligands (orange) and S290G ligands (green) are overlaid and show the ligand movements correlated with altered interactions in the active site.

Asp426 to N3 of CB3717. Figure 4 highlights the lost and gained interactions in the S290G active site.

Ligand Disorder in the TS Mutant Enzymes. The fact that ligand orientation is very similar for all three TS active site mutants, yet the rate decrease is more drastic for S290G, implies that there is another parameter playing a role in catalysis. Differences between S290G- and A287F-containing structures, including the lack of complete $F_o - F_c$ electron density (at 2.5σ) for CB3717 in S290G and decreased protein interactions at the folate tail in S290G, imply that the tail is more disordered in the severely affected mutant. As a means to assess possible differences in ligand flexibility between the mutant enzymes, the disorder of TS ligands was assessed by temperature-factor (*B*-factor) comparison. As shown in Table 4, while the disorder of the ligands in monomer B was nearly identical for all three mutants, the *B*-factors for CB3717 in monomer A were increased to a greater degree in S290G than in the other mutants. Specifically, the glutamate tail of CB3717 in monomer A of the S290G structure is significantly higher than in either A287F or A287F/S290G, by roughly 15 Å^2. The *p*-aminobenzoate group of CB3717, which includes the catalytically pertinent propargyl CP1, is also more disordered in S290G, again by about 10−15 Å^2. The quinazoline head of the folate, as well as dUMP, shows only small difference in flexibility. The folate differences are significant, as evidenced by the fact that the average *B*-factors for the individual TS monomers of both A287F and A287F/S290G are within 5 Å^2 of S290G, with A287F/S290G actually higher.

Conserved Water Network. It is well characterized that a strongly conserved water network coordinated by key residues in TS plays a role in catalysis and substrate positioning (*28, 29*). With the finding here that the ligands in the mutant enzyme active sites have an altered orientation, we investigated whether the water network was also altered.

The first major observation made when comparing the water networks is that, while the two conserved waters occupy similar spaces in WT and A287F, there was no electron density found for waters near these positions in monomer A of S290G. Both waters are present in A287F (Figure S1 of the Supporting Information). The position of Asn434, which coordinates the waters and hydrogen bonds to dUMP, is altered in the mutants. The hydrogen bond distance between the residue and dUMP is increased, and the hydrophobic interaction with both ligands is lost (Table 3). Density for these waters was present in monomer B of S290G, which showed similar movements for the coordinating residues in monomer A (Figure S1).

DISCUSSION

The mutations of residues 287 and 290 of *Ch*TS back to the classical phenylalanine and glycine, respectively, provide an opportunity to study the direct physical impact of two residues in the folate tail-binding region. The resulting study allows for specific information on thymidylate synthesis in *C. hominis*, as well as general principles applicable to the well-studied enzyme. While we would always caution the use of crystal structures alone in interpreting biochemical effects, the thorough kinetic analysis presented previously provides a good foundation for validating structural conclusions.

One of the main observations from all three mutants (S290G, A287F, A287F/S290G) with comparison to WT is that interactions at the folate tail-binding region, while limited in number, direct long-range effects throughout the active site (Figure 2A). Both the folate analogue CB3717 and the more remote substrate dUMP have multiple active site residue interactions that are dependent on the tail-binding residues. Small changes in positioning of TS ligands in response to mutations have been well documented before, and proper substrate positioning is known to be crucial for normal TS activity (*28, 30–32*). In the case of this *Ch*TS enzyme, Ser290 and Ala287 are able to modulate the enzyme active site further to obtain a dramatically increased catalytic efficiency.

It appears that the enhanced catalytic efficiency in *Ch*TS is due to two separate effects. Since all three mutant enzymes display the same distance increase between the catalytic atoms for methyl transfer and the loss of the hydrogen bond between O3′ of dUMP and N3 of the folate analogue, ligand positioning likely accounts for part of the catalytic decrease in efficiency. Additional evidence comes from the fact that some residues known to be crucial for TS activity, for instance the catalytic Cys402 and the water-coordinating Asn434, are among the protein−ligand interactions that are altered. The altered position of Cys402 with respect to dUMP, for example, might be either a defect responsible for the decreased catalytic rate or a metric of the misorientation of the ligands. The fact that the ligand positioning, including the catalytic distances and loss of interligand hydrogen bond, approaches that of the classical slow TS enzymes like human and *E. coli* (Figure 5), makes it more convincing that ligand positioning is at least partly responsible. The common result of the two mutated residues is the loss of the Ser290 hydrogen bond to the CB3717 folate tail. This loss in the S290G mutant is expected, but the A287F mutant is more surprising; Phe287 orders the carboxylate of the folate tail just enough so that the Ser290 hydrogen bond is unable to form. One abolished hydrogen bond at an extreme end of the active site seems to lead to long-range effects in the positioning of the ligands. The results imply that, in this active site, proper interactions at the tail end allow the substrates to form a hydrogen bond that optimally orients the active site for increased catalytic production. The loss of three protein−ligand hydrogen bonds (but gain of four additional bonds at other positions) in S290G emphasizes that the ligands indeed move and occupy slightly different, yet stably bound and discrete substrate pockets.

Table 4: Ligand Temperature Factors (Å) for Monomers A and B of S290G and A287F

			whole ligand		CB3717 moieties		
monomer	mutant enzyme	monomer *B*-factor	CB3717 average	dUMP average	glutamate tail	PABA	quinazoline
A	S290G	51	77	59	86	78	71
	A287F	45	67	56	71	63	68
	double	56	67	59	70	68	63
B	S290G	40	53	43	60	51	50
	A287F	36	53	42	62	51	50
	double	49	54	54	57	50	54

However, the distance change does not complete the story, as it is apparent that both mutants containing a phenylalanine at position 287 (A287F, A287F/S290G) are able to partially compensate the activity loss. Interestingly, it seems that a phenylalanine at either the traditional "down" position (A287F/S290G) or the novel "up" position (A287F) can equally regain some activity (Figure 2B); all kinetic parameters are identical for A287F and the double mutant (*6*). The only difference between the structures of S290G and the two mutants with A287F lies in the asymmetry of the TS dimer. In the more open monomer A, the S290G mutant seems to have increased folate (especially folate-tail) flexibility compared to the two mutants with a Phe287. This is also supported by the protein−ligand contacts, where monomer A of A287F and A287F/S290G displays an increase in contacts from CB3717 to Leu429, and the folate tail-binding residues (287, Phe433, and Ile315) versus S290G. The fact that the loss of these ligand contacts is only seen in monomer A, the partially closed conformer of the active TS dimer, implies that S290G has a specific catalytic impairment *before* the monomer is in the fully closed conformation. Presumably, the increased ligand flexibility in the open monomer makes it more difficult for the enzyme to close the active site during its transition to an active catalytic state. This implies that, without the added interaction at the folate tail, the S290G enzyme is unable to properly order and orient the ligands for optimal transition to the fully closed state. Indeed, the rate of conformational change preceding catalysis in the TS mechanism in S290G was shown to be almost 100-fold slower than WT, whereas A287F and A287F/S290G recover almost all of this loss (*6*).

Taken together, we propose a model for rate enhancement of the *Ch*TS domain in which both ligand positioning and flexibility play a role. A protein−ligand interaction at the folate tail, whether it be a hydrogen bond with Ser290 or van der Waals interaction with either conformation of Phe287, is necessary to properly orient the ligands in the partially closed state to undergo a normal conformational change to the active closed state. However, it is only in the context of the Ser290 hydrogen bond to the folate tail, which is necessary to position the ligands close enough to each other to form the dUMP-CB3717 hydrogen bond, that the full catalytic enhancement is achieved. The A287F mutant is particularly important, as it demonstrates that the nonclassical change of Gly290 to Ser290 alone cannot effect the full rate enhancement, and the additional change of the classical Phe287 to an alanine is required to allow for Ser290 to exert its full effect on the active site. The fact that the rate-limiting step in both WT *Ch*TS and the conserved, slower TS species is hydride transfer implies that close positioning of the ligands is also important for the hydride transfer step.

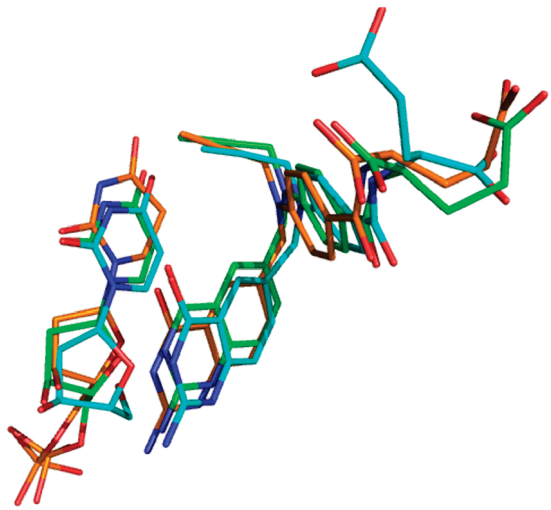

FIGURE 5: Overlay of TS ligands from WT (orange), S290G (green), and *E. coli* (gray) thymidylate synthase.

When comparing the parasite enzymes to the slower *E. coli* and human enzymes, it is interesting to note that the mutant that has comparable *activity* to the slower enzymes is S290G. This is somewhat unexpected, as the mutant that is comparable in *sequence* to the slow enzymes is actually the double mutant A287F/S290G, where both residues are the conserved amino acids. While substrate positioning is similar, consistent with the lack of a Ser290-to-folate hydrogen bond, there are differences in hydrophobic contacts. It is known that tail-binding residues show conformational differences in different species and in the presence of various inhibitors, while still maintaining similar contacts (*33, 34*). However, an analysis of *E. coli* TS (*35*) (PDB ID 1TRG) protein−ligand interactions reveals that there are actually far fewer contacts with the folate tail than in A287F (which has comparable activity to the double mutant). His51 (Phe287) makes no contact at all with the folate tail, and Ile79 (Ile315) makes only half of the interactions that it does in A287F. Additionally, Phe433, which contacts the *p*-aminobenzoate moiety, makes fewer contacts than in A287F. In fact, these tail-binding residue interactions much more closely resemble those in the slower S290G parasite enzyme. This comparison, from an enzyme species other than *C. hominis*, again displays a correlation between slower enzyme activity and lack of folate tail stabilizing interactions.

It is important to note that the changes in ligand positioning and folate tail interactions are pertinent for rates of catalysis, and not simply binding, since both steady-state and single-enzyme turnover chemical rates were affected similarly (Table 1). In fact, while the folate substrate CH_2H_4folate shows differential binding affinity for the A287F mutants and the S290G mutant, the folate analogue CB3717 shows

little alteration in affinity for the enzymes. The loss and gain of interactions in the active site argue for stably bound folate in each enzyme and perhaps emphasize the more subtle role of the folate tail-binding residues in folate ordering during the conformational change preceding catalysis, reflected in the kinetics (*6*).

The position of Phe287 in our A287F structure is of particular interest. Along with extracting the importance of the Ser290−CB3717 hydrogen bond, it is the first time that this rotamer has been observed for the conserved phenylalanine at this position. It should be noted that high-resolution structures of *E. coli* TS show His51 (comparable to Phe287) in multiple conformations, one of which is in the "up" position, although it is farther from the active site than Phe287 by almost 2 Å at the γ carbons, and not interacting with the folate tail (*36*). Additionally, we only observed the phenylalanines in the one conformation shown for each structure.

The altered water network in S290G and A287F mutants provides a clue that there are significant changes in the active site. The largest change in S290G, lack of good density for both conserved waters in monomer A, implies the more dynamic nature of that partially closed active site. Perhaps the most important point here is the altered distance between Asn434 and O4 of dUMP in both mutant structures. It has been shown previously that this interaction is important for proper alignment of substrates and charge stabilization on dUMP during covalent intermediate formation (*1, 28, 37*). The kinetic analysis of S290G showed that, in fact, the rate of this intermediate formation was decreased so much so that it became the limiting step in the overall catalytic mechanism (*6*). These data validate that the structural changes seen, specifically at dUMP, are important in assigning mutant enzyme effects, and this change may in fact be the ultimate effect leading to decreased steady-state activity in the mutants of Ser290 and Ala287.

This structural analysis combined with the previous kinetic analysis explains the importance of residues Ser290 and Ala287 for optimal *Ch*TS function. This validates the folate tail-binding region as a target for drug design against *C. hominis*. Two major obstacles in the design of effective therapeutic agents are host toxicity and the emergence of resistant forms of the targeted enzyme. The *C. hominis* folate tail-binding residues provide an opportunity to minimize both. Inhibitors designed to make specific interactions with Ser290 and Ala287 (glycine and phenylalanine, respectively, in the human TS enzyme) should impart some level of parasite species specificity. Additionally, the demonstrated importance of these two residues in *Ch*TS activity would make it unlikely that they would be mutated in an effort to decrease drug binding, thereby limiting a major mode of pathogen drug resistance. Molecular modeling studies are underway to determine inhibitors that preferentially bind *Ch*TS versus human TS.

ACKNOWLEDGMENT

We thank Robert Sweet, Howard Robinson, Sal Sclafani, Stu Myers, Rick Jackimowicz, and the entire staff at Beamlines X25 and X29 of the National Synchrotron Light Source at Brookhaven National Laboratory for their gracious technical help. We also thank Dr. Yoonsang Cho for helpful discussions.

SUPPORTING INFORMATION AVAILABLE

Two figures depicting the comparison of the conserved water network in the wild-type, S290G, and A287F enzymes. This material is available free of charge via the Internet at http://pubs.acs.org.

REFERENCES

1. Carreras, C. W., and Santi, D. V. (1995) The catalytic mechanism and structure of thymidylate synthase. *Annu. Rev. Biochem. 64*, 721–762.
2. Benkovic, S. J., and Hammes-Schiffer, S. (2003) A perspective on enzyme catalysis. *Science 301*, 1196–1202.
3. Santi, D. V., McHenry, C. S., and Sommer, H. (1974) Mechanism of interaction of thymidylate synthetase with 5-fluorodeoxyuridylate. *Biochemistry 13*, 471–481.
4. Atreya, C. E., and Anderson, K. S. (2004) Kinetic Characterization of Bifunctional Thymidylate Synthase-Dihydrofolate Reductase (TS-DHFR) from Cryptosporidium hominis: A Paradigm Shift for TS Activity and Channeling Behavior. *J. Biol. Chem. 279*, 18314–18322.
5. Vasquez, J. R., Gooze, L., Kim, K., Gut, J., Petersen, C., and Nelson, R. G. (1996) Potential antifolate resistance determinants and genotypic variation in the bifunctional dihydrofolate reductase-thymidylate synthase gene from human and bovine isolates of Cryptosporidium parvum. *Mol. Biochem. Parasitol. 79*, 153–165.
6. Doan, L. T., Martucci, W. E., Vargo, M. A., Atreya, C. E., and Anderson, K. S. (2007) Nonconserved Residues Ala287 and Ser290 of the Cryptosporidium hominis Thymidylate Synthase Domain Facilitate Its Rapid Rate of Catalysis. *Biochemistry 46*, 8379–8391.
7. O'Neil, R. H., Lilien, R. H., Donald, B. R., Stroud, R. M., and Anderson, A. C. (2003) Phylogenic classification of protozoa based on the structure of the linker domain in the bifunctional enzyme, dihydrofolate reductase-thymidylate synthase. *J. Biol. Chem. 278*, 52980–52987.
8. Anderson, A. C., O'Neil, R. H., Surti, T. S., and Stroud, R. M. (2001) Approaches to solving the rigid receptor problem by identifying a minimal set of flexible residues during ligand docking. *Chem. Biol. 8*, 445–457.
9. Anderson, A. C., Perry, K. M., Freymann, D. M., and Stroud, R. M. (2000) The crystal structure of thymidylate synthase from Pneumocystis carinii reveals a fungal insert important for drug design. *J. Mol. Biol. 297*, 645–657.
10. Almog, R., Waddling, C. A., Maley, F., Maley, G. F., and Van Roey, P. (2001) Crystal structure of a deletion mutant of human thymidylate synthase Delta (7−29) and its ternary complex with Tomudex and dUMP. *Protein Sci. 10*, 988–996.
11. Kamb, A., Finer-Moore, J. S., and Stroud, R. M. (1992) Cofactor triggers the conformational change in thymidylate synthase: implications for an ordered binding mechanism. *Biochemistry 31*, 12876–12884.
12. Dillingham, R., Lima, A., and Guerrant, R. (2002) Cryptosporidiosis: epidemiology and impact. *Microbes Infect. 4*, 1059–1066.
13. Otwinowski, Z., and Minor, W. (1997) Processing of X-Ray Diffraction Data Collected in Oscillation Mode. *Methods Enzymol. 276*, 307–326.
14. Collaborative Computational Project, N. (1994) The CCP4 Suite: Programs for Protein Crystallography. *Acta Crystallogr., Sect. D: Biol. Crystallogr. 50*, 760–763.
15. Murshudov, G. N., Vagin, A. A., and Dodson, E. J. (1997) Refinement of macromolecular structures by the maximum-likelihood method. *Acta Crystallogr., Sect. D: Biol. Crystallogr. 53*, 240–255.
16. Jones, T. A., Zou, J. Y., Cowan, S. W., and Kjeldgaard, M. (1991) Improved methods for building protein models in electron density maps and the location of errors in these models. *Acta Crystallogr. A 47* (Part 2), 110–119.
17. Emsley, P., and Cowtan, K. (2004) Coot: model-building tools for molecular graphics. *Acta Crystallogr., Sect. D: Biol. Crystallogr. 60*, 2126–2132.
18. Brunger, A. T., Adams, P. D., Clore, G. M., DeLano, W. L., Gros, P., GrosseKunstleve, R. W., Jiang, J. S., Kuszewski, J., Nilges, M., Pannu, N. S., Read, R. J., Rice, L. M., Simonson, T., and

Warren, G. L. (1998) Crystallography & NMR system: A new software suite for macromolecular structure determination. *Acta Crystallogr., Sect. D: Biol. Crystallogr. 54*, 905–921.
19. Finer-Moore, J. S., Montfort, W. R., and Stroud, R. M. (1990) Pairwise specificity and sequential binding in enzyme catalysis: thymidylate synthase. *Biochemistry 29*, 6977–6986.
20. Bystroff, C., and Kraut, J. (1991) Crystal structure of unliganded Escherichia coli dihydrofolate reductase. Ligand-induced conformational changes and cooperativity in binding. *Biochemistry 30*, 2227–2239.
21. Anderson, A. C., O'Neil, R. H., DeLano, W. L., and Stroud, R. M. (1999) The structural mechanism for half-the-sites reactivity in an enzyme, thymidylate synthase, involves a relay of changes between subunits. *Biochemistry 38*, 13829–13836.
22. Johnson, E. F., Hinz, W., Atreya, C. E., Maley, F., and Anderson, K. S. (2002) Mechanistic characterization of Toxoplasma gondii thymidylate synthase (TS-DHFR)-dihydrofolate reductase. *J. Biol. Chem. 277*, 43126–43136.
23. Jackson, M., Beahm, R., Duvvuru, S., Narasimhan, C., Wu, J., Wang, H.-N., Philip, V. M., Hinde, R. J., and Howell, E. E. (2007) A preference for edgewise interactions between aromatic rings and carboxylate anions: the biological relevance of anion-quadrupole interactions. *J. Phys. Chem. B 111*, 8242–8249.
24. Guallar, V., and Borrelli, K. W. (2005) A binding mechanism in protein-nucleotide interactions: Implication for U1A RNA binding. *Proc. Natl. Acad. Sci. U.S.A. 102*, 3954–3959.
25. Birdsall, D. L., Finer-Moore, J., and Stroud, R. M. (2003) The only active mutant of thymidylate synthase D169, a residue far from the site of methyl transfer, demonstrates the exquisite nature of enzyme specificity. *Protein Eng. 16*, 229–240.
26. Montfort, W., Perry, K., Fauman, E., Finer-Moore, J., Maley, G., Hardy, L., Maley, F., and Stroud, R. (1990) Structure, multiple site binding, and segmental accommodation in thymidylate synthase on binding dUMP and an anti-folate. *Biochemistry 29*, 6964–6977.
27. Wallace, A. C., Laskowski, R. A., and Thornton, J. M. (1995) LIGPLOT: a program to generate schematic diagrams of protein-ligand interactions. *Protein Eng. 8*, 127–134.
28. Finer-Moore, J. S., Liu, L., Birdsall, D. L., Brem, R., Apfeld, J., Santi, D. V., and Stroud, R. M. (1998) Contributions of orientation and hydrogen bonding to catalysis in Asn229 mutants of thymidylate synthase. *J. Mol. Biol. 276*, 113–129.
29. Sage, C. R., Rutenber, E. E., Stout, T. J., and Stroud, R. M. (1996) An essential role for water in an enzyme reaction mechanism: the crystal structure of the thymidylate synthase mutant E58Q. *Biochemistry 35*, 16270–16281.
30. Birdsall, D. L., Huang, W., Santi, D. V., Stroud, R. M., and Finer-Moore, J. (1998) The separate effects of E60Q in Lactobacillus casei thymidylate synthase delineate between mechanisms for formation of intermediates in catalysis. *Protein Eng. 11*, 171–183.
31. Fritz, T. A., Liu, L., Finer-Moore, J. S., and Stroud, R. M. (2002) Tryptophan 80 and leucine 143 are critical for the hydride transfer step of thymidylate synthase by controlling active site access. *Biochemistry 41*, 7021–7029.
32. Sage, C. R., Michelitsch, M. D., Stout, T. J., Biermann, D., Nissen, R., Finer-Moore, J., and Stroud, R. M. (1998) D221 in thymidylate synthase controls conformation change, and thereby opening of the imidazolidine. *Biochemistry 37*, 13893–13901.
33. Jones, T. R., Webber, S. E., Varney, M. D., Reddy, M. R., Lewis, K. K., Kathardekar, V., Mazdiyasni, H., Deal, J., Nguyen, D., Welsh, K. M., Webber, S., Johnston, A., Matthews, D. A., Smith, W. W., Janson, C. A., Bacquet, R. J., Howland, E. F., Booth, C. L., Herrmann, S. M., Ward, R. W., White, J., Bartlett, C. A., and Morse, C. A. (1997) Structure-based design of substituted diphenyl sulfones and sulfoxides as lipophilic inhibitors of thymidylate synthase. *J. Med. Chem. 40*, 677–683.
34. Sotelo-Mundo, R. R., Ciesla, J., Dzik, J. M., Rode, W., Maley, F., Maley, G. F., Hardy, L. W., and Montfort, W. R. (1999) Crystal structures of rat thymidylate synthase inhibited by Tomudex, a potent anticancer drug. *Biochemistry 38*, 1087–1094.
35. Stout, T. J., Sage, C. R., and Stroud, R. M. (1998) The additivity of substrate fragments in enzyme-ligand binding. *Structure 6*, 839–848.
36. Newby, Z., Lee, T. T., Morse, R. J., Liu, Y., Liu, L., Venkatraman, P., Santi, D. V., Finer-Moore, J. S., and Stroud, R. M. (2006) The role of protein dynamics in thymidylate synthase catalysis: variants of conserved 2′-deoxyuridine 5′-monophosphate (dUMP)-binding Tyr-261. *Biochemistry 45*, 7415–7428.
37. Matthews, D. A., Appelt, K., Oatley, S. J., and Xuong, N. H. (1990) Crystal structure of Escherichia coli thymidylate synthase containing bound 5-fluoro-2′-deoxyuridylate and 10-propargyl-5,8-dideazafolate. *J. Mol. Biol. 214*, 923–936.

BI800466Z